Data-driven Modeling and Feedback Tracking Control of the Toroidal Rotation Profile for Advanced Tokamak Scenarios in DIII-D

W. Wehner, C. Xu, E. Schuster, D. Moreau, D. Mazon, M.L. Walker, D.A. Humphreys and Y. In

Abstract— **First-principle tokamak plasma predictive models based on flux averaged transport equations often yield complex expressions not suitable for real time control implementations. Addition of turbulent transport phenomena further encumbers these models with transport coefficients that must be determined experimentally and the interdependences between parameters must be accounted for with ad hoc assumptions. As an alternative to first principle modeling, data-driven modeling techniques involving system identification have the potential to obtain practical, low complexity, dynamic models without the need for ad hoc assumptions. This paper considers the evolution of the toroidal rotation profile in response to the heating and current drive (H&CD) systems. Experiments are conducted during plasma current flattop, in which the actuators are modulated in open-loop to obtain data for the model identification. The rotation profile is discretized in the spatial coordinate by Galerkin projection. Then a linear state space model is generated by the prediction error method (PEM) to relate the rotation profile to the actuators according to a least squares fit. An optimal tracking controller is proposed to regulate the rotation profile to a desired reference trajectory.**

I. Introduction

For sustained high-gain fusion operation, tokamak plasmas must exhibit high energy confinement, defined as the time required for the input energy to dissipate from the plasma. Experiments have shown that high plasma rotation, i.e., bulk fluid rotation around the tokamak, can have a significant impact on the confinement time by suppressing energy and particle transport to the wall. This effect is somewhat intuitive, considering the fact that a large portion of energy degradation stems from turbulence, and a gradient in the rotation velocity will suppress the development of turbulent flow across the plasma. Since the tokamak wall does not move, a velocity gradient will exist between the plasma and the wall, so, the larger the rotation, the larger the rotation gradient. Additionally, plasma rotation can minimize the effect of error fields that can influence the magnetic topology and excite tearing modes. A rapidly rotating plasma will increase the effective frequency of the error field in the plasma frame and reduce the depth of its penetration. Tearing modes rotating with the plasma velocity will thus be substantially suppressed in a rotating plasma. This same reasoning applies to resistive wall mode instabilities as well [1], [2].

This work was supported by the NSF CAREER award program (ECCS-0645086) and the U.S. Department of Energy (DE-FG02-09ER55064, DE-FG02-92ER54141, DE-FC02-04ER54698 and DE-FG02-06ER84442). W. Wehner and E. Schuster (schuster@lehigh.edu) are with the Department of Mechanical Engineering and Mechanics, Lehigh University, Bethlehem, PA 18015, USA. M. Walker and D. Humphreys are with General Atomics, P.O. Box 85608, San Diego, CA 92186, USA. Y. In is with FAR-TECH, Inc., 10350 Science Center Drive, San Diego, CA, 92121 USA. D. Moreau is with CEA, IRFM, 13108 Saint-Paul-lez-Durance, France

Mathematical modeling of plasma transport phenomena with sufficient complexity to capture the dominant dynamics is critical for plasma control design. Transport theories (classical, neoclassical and anomalous) even under restrictive assumptions, produce strongly nonlinear models based on partial differential equations (PDEs). The complexity of these models often makes them impractical for control design since it is very challenging, if not impossible, to synthesize compact and reliable control strategies based on these complicated mathematical models. As an alternative, data-driven modeling techniques, including system identification [3] and data assimilation [4], have the potential to obtain practical, low-complexity, dynamic models useful for implementing relatively simple control design problems for tokamaks.

Data-driven modeling techniques have been successfully used in the past to model plasma transport dynamics for active control design in nuclear fusion reactors (see, e.g., [5]). System identification using input/output (I/O) diagnostic data has been used to model the current profile dynamics in ASDEX Upgrade [6]. In the JET tokamak [7], a two-time-scale linear system has been used to describe the dynamics of the magnetic and kinetic profiles around certain quasi-steady-state trajectories, where system matrices can be identified from experimental data. In the L-mode discharges of the JT-60U tokamak [8], diffusive and nondiffusive coefficients of the momentum transport equation of the toroidal rotation profile dynamics have been estimated from transient data obtained by modulating the momentum source.

This paper aims at developing an input output response model, suitable for real-time profile control, for the toroidal rotation in DIII-D during AT scenarios. A linear time invariant model is synthesized using system identification methods. Finally, the model is used for an optimal control synthesis to regulate the rotation profile to a desired reference. Section II describes the system identification process and using this process a model relating the rotation profile to the neutral beams, current drives, and the toroidal loop voltage is obtained. In section III we propose an optimal control tracking method for following a desired velocity profile. Section IV considers simulations of reference profile tracking for an initially disturbed and an initially undisturbed system. It is concluded in section V that the response of the toroidal rotation profile in DIII-D to specific actuators can be satisfactorily identified from a small set of experiments. This provides, for control purposes, readily available models which are far less complex than those obtained from first principle modelling and thus better suited for control design.

II. Experimental Method and System identification on DIII-D

By taking the surface average over the magnetic flux surfaces, plasma transport equations can be represented by one dimensional nonlinear parabolic PDEs whose variables are dependent on both time t and the normalized radius $\hat{\rho}$. Around certain given trajectories, the nonlinear PDEs can be linearized as

$$\frac{\partial x(\hat{\rho},t)}{\partial t} = \mathcal{A}(\hat{\rho})x(\hat{\rho},t) + \mathcal{B}(\hat{\rho})u(t) + \mathcal{K}(\hat{\rho},t)e(\hat{\rho},t), \quad (1)$$

where $x(\hat{\rho},t)$ represents the collection of physical variables, e.g., the poloidal magnetic flux, $\psi(\hat{\rho},t)$, the toroidal velocity $V_\phi(\hat{\rho},t)$, the ion and electron temperatures $T_{i,e}(\hat{\rho},t)$. The variable $u(t)$ represents external and auxiliary inputs, such as various current drives (ECCD), neutral beam injection (NBI), electron cyclotron resonance heating (ECRH), and the plasma boundary loop voltage (V_{ext}). The variables $\mathcal{A}(\hat{\rho})$, $\mathcal{B}(\hat{\rho})$, and $\mathcal{K}(\hat{\rho})$ are infinite dimensional operators. The system outputs (2) can be measured via various diagnostic systems

$$y(\hat{\rho},t) = \mathcal{C}(\hat{\rho})x(\hat{\rho},t) + e(\hat{\rho},t), \quad (2)$$

where $\mathcal{C}(\hat{\rho})$ is the observation operator and $e(\hat{\rho},t)$ is the observation noise field. The infinite dimensional system can be approximated by projecting the distributed variable $y(\hat{\rho},t)$ onto a basis function space. In this paper a discretized system is generated by Galerkin projection and it is simply assumed that by increasing the number of trial basis functions the discrete system would converge towards the infinite dimensional differential system. The Galerkin projection of a generic dynamical variable, $y(\hat{\rho},t)$, reads:

$$y(\hat{\rho},t) \approx \sum_{i=1}^{N} G_{y,i}(t)b_i(\hat{\rho}), \quad (3)$$

where $b_i(\hat{\rho})$ are the basis functions. In this paper the basis functions are piece-wise linear functions as shown in Fig. 1 with $i = 1,2,...N$. The expansion coefficients, $G_{y,i}(t)$, will be called Galerkin coefficients and the vector array containing the Galerkin coefficients of the variable $y(\hat{\rho},t)$ will simply be named $Y(t)$. To determine the Galerkin coefficients, we multiply both sides of the expansion equation (3) with any basis function $b_j(\hat{\rho})$, $j = 1,2,...N$ and integrate over the spatial coordinate to obtain,

$$\int_0^1 y(\hat{\rho},t)b_j(\hat{\rho})d\hat{\rho} = \int_0^1 \Big[\sum_{i=1}^{N} G_{y,i}(t)b_i(\hat{\rho})\Big]b_j(\hat{\rho})d\hat{\rho}, \quad (4)$$

for $j = 1,2,...N$. If the basis functions are orthonormal, i.e. $\int_0^1 b_i(\hat{\rho})b_j(\hat{\rho})d\hat{\rho} = \delta_{ij}$, then the coefficients $G_{y,i}$ can be computed explicitly. Otherwise the coefficients are obtained by the matrix equation.

$$\begin{bmatrix} q_1 \\ q_2 \\ \vdots \\ q_N \end{bmatrix} = \begin{bmatrix} m_{11} & m_{12} & \dots & m_{1n} \\ m_{21} & m_{22} & \dots & m_{2n} \\ \vdots & \vdots & \ddots & \vdots \\ m_{n1} & m_{n2} & \dots & m_{nn} \end{bmatrix} \begin{bmatrix} G_{y,1} \\ G_{y,2} \\ \vdots \\ G_{y,N} \end{bmatrix} \quad (5)$$

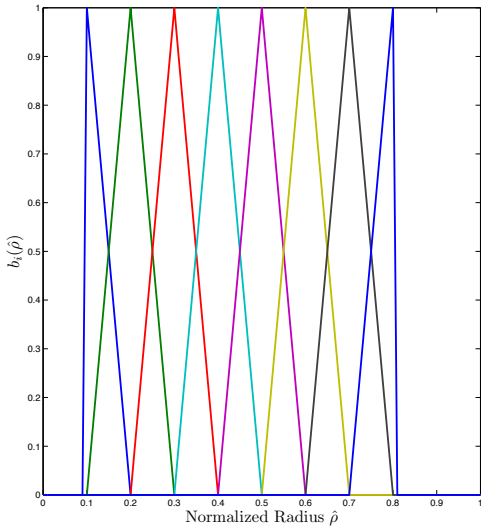

Fig. 1. Piece-wise linear functions $b_i(\hat{\rho})$, used for the expansion of $V_{phi}(\hat{\rho})$

where m_{ij} is the inner product of b_i and b_j, i.e., $\int_0^1 b_i(\hat{\rho})b_j(\hat{\rho})d\hat{\rho}$ and q_j is the inner product between $y(\hat{\rho},t)$ and $b_j(\hat{\rho})$, i.e., $\int_0^1 y(\hat{\rho},t)b_j(\hat{\rho})d\hat{\rho}$. After this discretization has been made, the lumped parameter version of the state space model is obtained, which reads:

$$\begin{array}{rcl} \frac{dX(t)}{dt} & = & AX(t) + Bu(t) + Ke(t), \\ Y(t) & = & CX(t) + e(t). \end{array} \quad (6)$$

where $u(t)$ are the inputs, e.g., neutral beam injection (NBI) power, electron cyclotron current drive (ECCD) power, and the loop voltage (V_{ext}). Then we seek a least squares fit of the discrete model of the system to experimental data.

To collect the data for system identification a number of discharges of an advanced tokamak scenario were run with identical ramp-up phases and during flattop various actuators were modulated around their reference values. Experiments were carried out in the loop voltage (V_{ext}) control mode (as opposed to current control) to avoid feedback in the response data from the primary circuit. The reference plasma (identical to shot #133103) state was that of a 0.9 MA AT scenario which had been optimized to combine non-inductive current fractions near unity with $3.5 < \beta_N < 3.9$, bootstrap current fractions larger than 65%, and $H_{98}(y,2) = 1.5$ [9]. Actuator modulations were applied from $t = 2.6$ s, i.e., after 1 s of 0.9 MA current flat top. At this time, in all discharges, the I_p and β_N controls were disabled and V_{ext} was enabled as an actuator. This ensures there is no feedback response in the system during data collection. The NBI and ECCD systems provided the heating and current drive sources for these experiments. Available beam-lines and gyrotrons were grouped to form, together with V_{ext}, five independent actuators: *i*- co-current NBI power (P_{CO}) *ii*- counter-current NBI power (P_{CNT}) *iii*- balanced NBI power (P_{BAL}) *iv*- total ECCD power from all gyrotrons in a fixed off-axis current drive configuration (P_{EC}), and *v*- V_{ext}. All actuators were modulated individually in open loop according to predefined waveforms while the other actuators

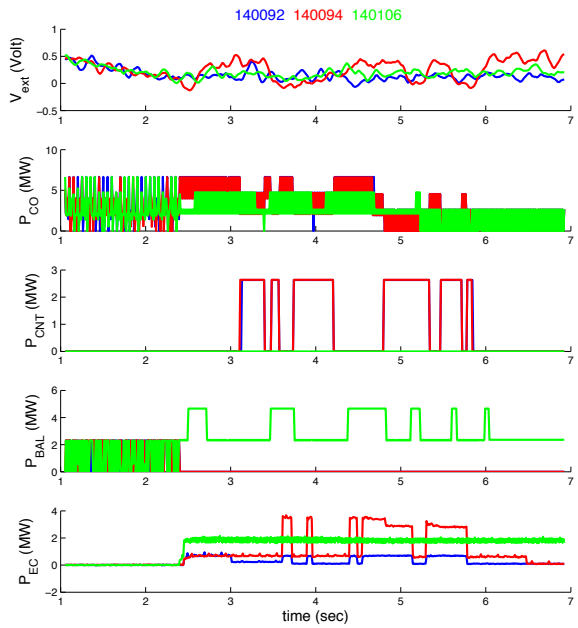

Fig. 2. Time evolution of V_{ext}, P_{CO}, P_{CNT}, P_{BAL}, and P_{EC} in DIII-D shots #140092, 140094, and 140106

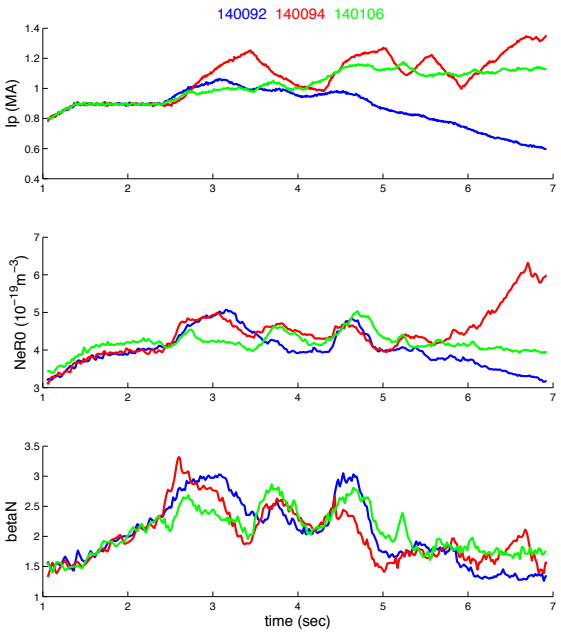

Fig. 3. Time evolution of β_N, N_eR_0, I_p in DIII-D shots #140092, 140094, and 140106

were kept constant and equal to those values used to produce the reference discharge. Power and loop voltage modulations resulted in dynamic variations of the plasma current between 0.7 and 1.2 MA. Fig. 2-3 display some typical modulations of the system inputs and of the plasma current I_p, line-averaged density N_eR_0, and the normalized pressure β_N.

System identification for the toroidal rotation profile $V_\phi(x,t)$ was carried out with 8 Galerkin coefficients computed at normalized radii $\hat{\rho} = 0.1, 0.2, ..., 0.8$, starting at $t =$ 2.6 s. Fig. 4-6 display some of the typical fits between the experimental data and the synthesized model, in these cases the model is compared to shots not used in the identification process. An offset has been subtracted to all the data sets so that the identification routine only handles datasets with zero average. Reasonable fits were obtained for most of the shots, including shots not used in the identification process. The fit between the original data $Y(t)$ and the reconstructed data $Y_m(t)$ is characterized by the parameter f,

$$f = 1 - \left[\frac{\sum_{k=1}^{N} [Y(t) - Y_m(t)]^2}{\sum_{k=1}^{N} [Y(t) - \langle Y \rangle]} \right], \tag{7}$$

where $f = 1$ (100%) is a perfect fit and $f = 0$ corresponds to a reconstructed data set equal to the mean of the measured data, $\langle Y \rangle$.

Several shots are used to generate the model (shot #140076, 140077, 140093, 140106, and 140107). Shot 140107 performs V_{ext} modulation, shots 140076, 140077, and 140106 provide modulation for the neutral beam groups, and 140093 includes modulation of the gyrotrons, to determine the effect of total ECCD power. We assume the input/output relation for any given shot is of the form

$$V_\phi = \bar{V}_\phi + \Delta V_\phi = \bar{G}(\bar{u}) + G\Delta u \tag{8}$$

where $\bar{G}$ represents the relationship between the reference input $\bar{u}$ and reference output $\bar{V}_\phi$. We simply subtract this reference value from our data set and consider only the left over dynamics $\Delta V_\phi = G\Delta u$. The reference value is subtracted out of each data set and the resulting dynamics are added together to perform the identification. The resulting dataset allows us to solve for the system

$$V'_\phi = Gu' \tag{9}$$

where $V'_\phi = \Delta V_{\phi,1} + \Delta V_{\phi,2} + ... + \Delta V_{\phi,N}$ and $u' = [\Delta u_1, \Delta u_2, ..., \Delta u_N]^T$, thus we can synthesize a model that incorporates all of the dynamics in the identification shots. An optimal $G(q)$ according to a least squares fit criterion is determined using the prediction error method (PEM) [3]. The PEM method calculates the matrices A, B, and C by the minimization of the norm V_N, which for a least squares fit is defined as

$$V_N(G) = \frac{1}{N} \sum_{k=1}^{N} \epsilon^2(k) \tag{10}$$

where $\epsilon(k)$, called the prediction error, is the difference between the measured output and the predicted output of the model.

$$\epsilon[k] = H^{-1}(q)(y[k] - G(q)u[k]) \tag{11}$$
$$y[k] = G(q)u[k] + H(q)\epsilon[k] \tag{12}$$
$$G(q) = C(qI - A)^{-1}B \tag{13}$$
$$H(q) = C(qI - A)^{-1}K + I \tag{14}$$

where q is the forward shift operator, i.e., $qu[k] = u[k+1]$ or $q^{-1}u[k] = u[k-1]$, and the matrices A, B, C, K represent the discrete time system,

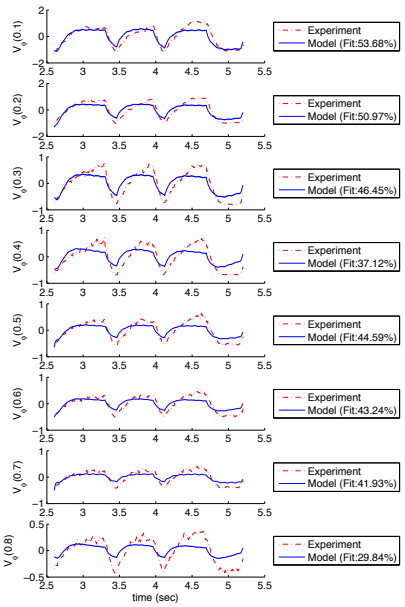

Fig. 4. Comparison between model (blue line) and measured (red dash) V_ϕ data (10^5 m/s) at $\hat{\rho} = 0.1, 0.2, ...0.8$ for DIII-D shot 140076.

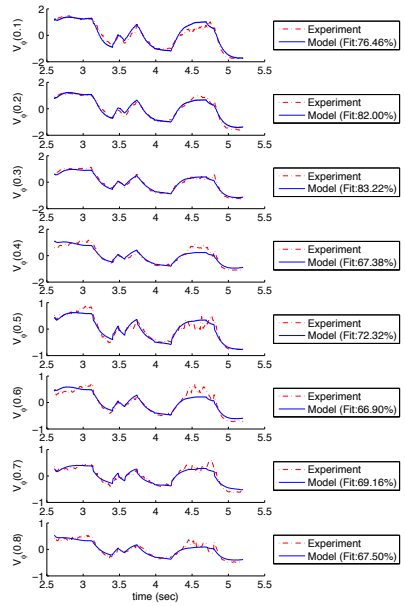

Fig. 5. Comparison between model (blue line) and measured (red dash) V_ϕ data (10^5 m/s) at $\hat{\rho} = 0.1, 0.2, ...0.8$ for DIII-D shot 140092.

$$x[k+1] = Ax[k] + Bu[k] + Ke[k] \quad (15)$$
$$y[k] = Cx[k] + e[k] \quad (16)$$

III. Discrete time linear quadratic tracking control

For a linear time invariant system described by the state equation

$$x[k+1] = Ax[k] + Bu[k] \quad (17)$$

and the output relation

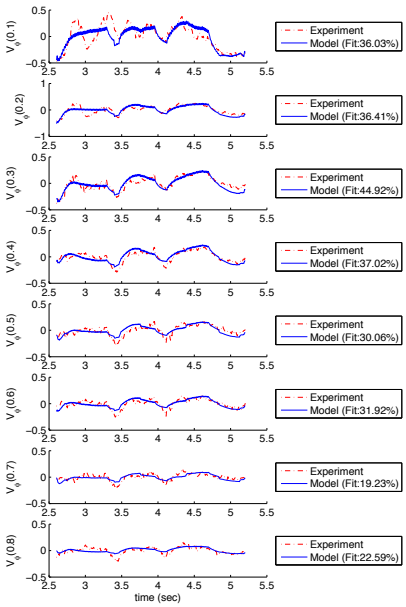

Fig. 6. Comparison between model (blue line) and measured (red dash) V_ϕ data (10^5 m/s) at $\hat{\rho} = 0.1, 0.2, ...0.8$ for DIII-D shot 140109.

$$y[k] = Cx[k] \quad (18)$$

The task of control synthesis is to find a feedback policy $u[k] = f(x[k])$ that minimizes the following cost functional J, i.e., find,

$$\min_u J = \frac{1}{2}\left(Cx[N] - z[N]\right)^T F \left(Cx[N] - z[N]\right) + \frac{1}{2}\sum_{k=1}^{N}\left\{ \left(Cx[k] - z[k]\right)^T Q \left(Cx[k] - z[k]\right) + u^T[k] R u[k] \right\} \quad (19)$$

where $x[k]$, $u[k]$, and $y[k]$ are n, r, and p order, state, control and output vectors, respectively. Also we assume F and Q are each $n \times n$ dimensional positive semidefinite symmetric matrices, and R is an $r \times r$ positive definite symmetric matrix. The initial condition is given as $x[k_0]$ and the final condition $x[k_f]$ is free with k_f fixed. We want the error $e[k] = y[k] - z[k]$ as small as possible with minimum control effort, where $z[k]$ is an n dimensional reference vector. By introducing the Lagrange multiplier $\lambda[k] \in \mathbb{R}^{n\times 1}$, we can define Hamiltonian functional of the tracking problem as

$$H[k] = \frac{1}{2}(Cx[k] - z[k])^T Q (Cx[k] - z[k]) + u[k]^T R u[k] + \lambda^T[k+1](Ax[k] + Bu[k]), \quad (20)$$

from which we obtain the optimal solution characterized by the following set of differential equations in the state x and costate λ,

$$x^*[k+1] = \frac{\partial H[k]}{\partial \lambda^*[k+1]} = Ax^*[k] + Bu^*[k], \quad (21)$$

$$\lambda^*[k] = \frac{\partial H[k]}{\partial x^*[k]} = A^T\lambda^*[k+1] + Vx^*[k] - Wz[k], \quad (22)$$

where $(\cdot)^*$ indicates the optimal value, $V = C^TQC$, and $W = C^TQ$. According to the principle of optimality,

$\partial H/\partial u = 0$, the optimal control law is given by

$$\frac{\partial H[k]}{\partial u^*[k]} = 0 \Rightarrow u^*[k] = -R^{-1}B^T\lambda^*[k+1], \quad (23)$$

with final condition

$$\lambda[N] = C^T FCx[N] - CFz[N]. \quad (24)$$

To obtain the closed-loop form, we assume a transformation bases on the form of the boundary condition

$$\lambda^*[k] = P[k]x^*[k] - g[k], \quad (25)$$

where the $n \times n$ matrix $P[k]$ and the $n \times 1$ vector $g[k]$ are to be solved off-line and backwards using the final condition. $P[k]$ is the nonlinear, matrix difference Ricatti equation and $g[k]$ is the linear, vector difference equation,

$$P[k] = A^T\left(P^{-1}[k+1] + E\right)^{-1}A + V, \quad (26)$$

$$g[k] = \Big\{A^T - A^T P[k+1]\Big(I + EP[k+1]\Big)^{-1} E^T\Big\}g[k+1] + Wz[k], \quad (27)$$

where $E = BR^{-1}B^T$ with boundary conditions

$$P[k_f] = C^T FC \quad (28)$$

$$g[k_f] = C^T Fz[N]. \quad (29)$$

Then using Eq. (25) to solve for the closed-loop optimal control law

$$u^*[k] = -L[k]x^*[k] + L_g[k]g[k+1], \quad (30)$$

where the feedback gain $L[k]$ and feed forward gain $L_g[k]$ are given by

$$L[k] = (R + B^T P(k+1)B)^{-1}B^T P[k+1]A, \quad (31)$$

$$L_g[k] = (R + B^T P[k+1]B)^{-1}B^T, \quad (32)$$

and the optimal state trajectory becomes

$$x^*[k+1] = (A - BL[k])x[k] + BL_g[k]g(k+1). \quad (33)$$

IV. Simulation Results

We present simulation results showing the effectiveness of the proposed optimal control algorithm applied to the identified model from section II. For this simulation study we consider a time interval $[t_0 = 0, t_N = 1.0$ s$]$ relative to an initial time $t_{init} = 2.6$ s in the experiment, i.e., $t_0 = 0$ in the simulations corresponds to $t_{init} = 2.6$ s in the experiment, 1 s after flattop when data collection for the system identification begins. In simulation, we consider two cases; *(i)* driving an initially disturbed system to zero (regulator control), and *(ii)* driving the system from zero to a desired profile (constant reference tracking). In each case the cost function weighting matrices are specified as follows; $F = 10I_n$, $Q = 100I_n$, and $R = 0.001I_r$ and the sampling period is $T_s = 0.01$ s.

Fig. 7-9 show the results of the initial disturbance rejection case. Here the initial condition is $Y_i(0) = [0.091\ 0.115\ 0.044\ -0.003\ -0.027\ -0.05\ -0.07\ -0.097]^T$.

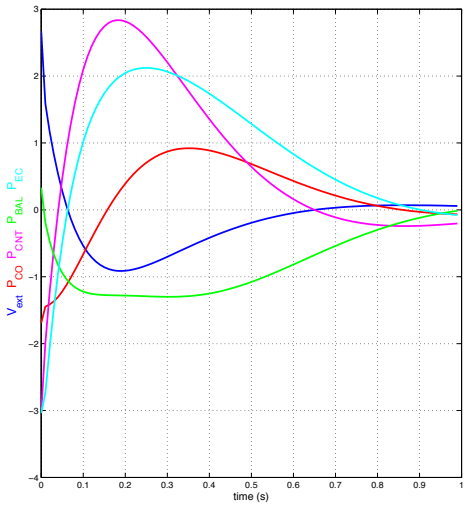

Fig. 7. Optimal tracking control inputs: V_{ext}, P_{CO}, P_{CNT}, P_{BAL}, and P_{EC} for the disturbance rejection case.

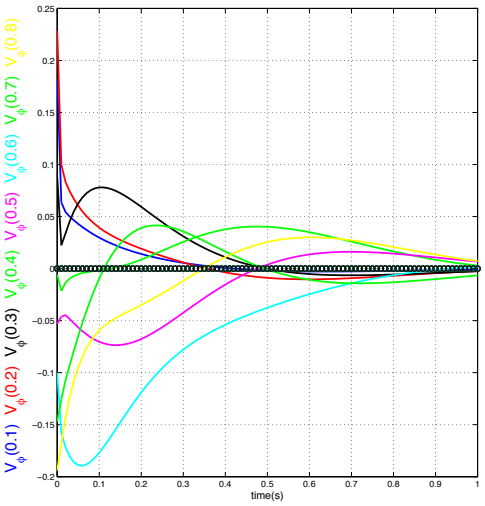

Fig. 8. Convergence of optimal tracking control for the disturbance rejection case ($V_\phi(0.1)$-$V_\phi(0.8)$). The black circles represents the reference for all the outputs.

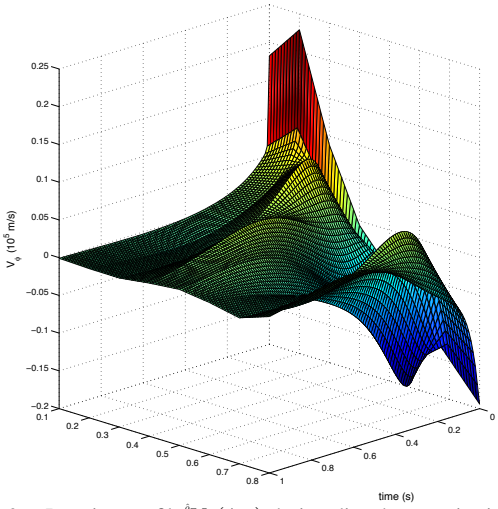

Fig. 9. Rotation profile ${}^{\hat{\rho}}V_\phi(\hat{\rho}, t)$ during disturbance rejection case.

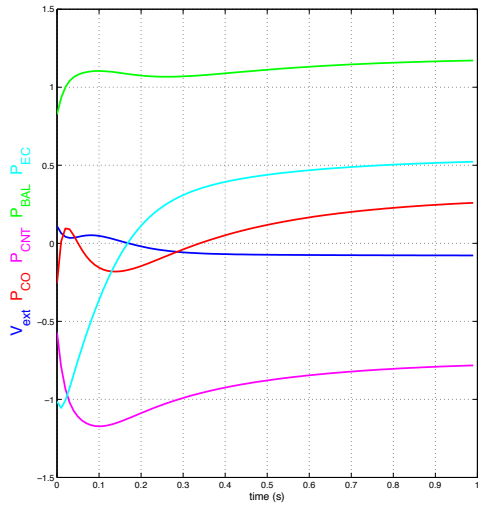

Fig. 10. Optimal tracking control inputs: V_{ext}, P_{CO}, P_{CNT}, P_{BAL}, and P_{EC} for the constant reference tracking case.

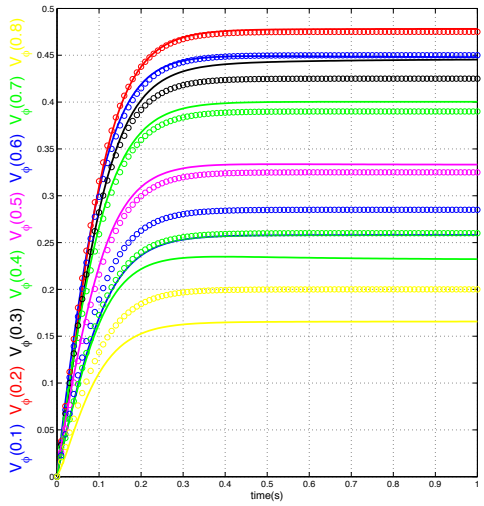

Fig. 11. Convergence of optimal tracking control for the constant reference tracking case ($V_\phi(0.1)$-$V_\phi(0.8)$). The lines are the outputs and the circles are the corresponding references.

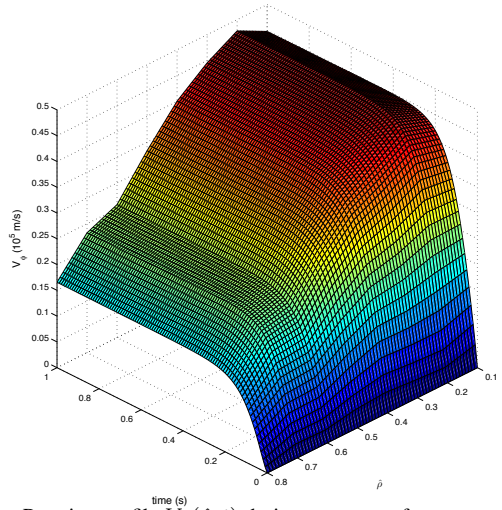

Fig. 12. Rotation profile $V_\phi(\hat{\rho}, t)$ during constant reference tracking case.

The control successfully drives the system to zero with all the states converging after about 0.9 s. The disturbance rejection represents the case in which the rotation profile has deviated from the desired shape (characterized by zero), the control is initiated and the profile is adjusted.

Fig. 10-12 show the results of the constant reference tracking case. Here the system starts at zero and is driven to a constant reference value $Y_i(N) = [0.450\ \ 0.475\ \ 0.400\ \ 0.350\ \ 0.325\ \ 0.300\ \ 0.275\ \ 0.20]^T$. To avoid fast dynamics in the system, the constant tracking reference is actually approximated as a hyperbolic tangent approaching, asymptotically the final value. Essentially this acts to slow the system down, but results in less overshoot. In this case the rotation is successfully sped up across the plasma with all the states fully converging after about 0.4 s. This case represents the situation in which it is desirable to speed up the rotation across the plasma. Note that the zero rotation value refers to some reference profile shape, not an absolute zero rotation.

V. Conclusions

In this paper we have developed a simplified linear model based on system identification methods for the profile evolution of the toroidal rotation profile in DIII-D. We have been able to generate reasonable model prediction of the rotation profile to modulations in the neutral beam injectors, the current drive power, and the external loop voltage by data driven techniques. An optimal tracking control is proposed for following a desired reference profile in closed-loop. Sufficient profile control using the optimal control method was also possible with feasible input power limits.

In the future we plan to incorporate the coupled dynamics between the rotation and current profiles into the model. The integration of rotation and current profiles into a single controller is particularly relevant to advanced tokamak scenarios in future devices such as ITER where the heating and current drive (H&CD) actuators will be quite constrained [7].

References

[1] M. DeBock, "Understanding and controlling plasma rotation in tokamaks," Ph.D. dissertation, Technische Universiteit Eindhoven, Eindhoven, jan 2007.

[2] Z. Lin, T. Hahm, W. Lee *et al.*, "Turbulent transport reduction by zonal flows: Massively parallel simulations," *Science*, vol. 281, no. 104007, pp. 1835–1837, 1998.

[3] L. Ljung, *System Identification: Theory for the User*. Prentice Hall PTR, 1999.

[4] B. Anderson and J. Moore, *Optimal Filtering*. Prentice Hall, 1979.

[5] P. Wang, *Distributed Parameter Systems: Modelling and Identification*. Berlin, Germany: Springer-Verlag, 1978.

[6] Y. S. Na, "Modelling of current profile control in tokamak plasmas," Ph.D. dissertation, Fakultat fur Physik: Technische Universitat Munchen, Munich, Germany, 2003.

[7] D. Moreau *et al.*, "A two time scale dynamic model approach for magnetic and kinetic profile control in advanced tokamak scenarios on JET," *Nucl. Fusion*, vol. 48, no. 106001, 2008.

[8] Y. Yoshida *et al.*, "Momentum transport and plasma rotation profile in toroidal direction in JT-60U L-mode plasmas," *Nucl. Fusion*, vol. 47, no. 8, pp. 856–863, 2007.

[9] C. Holcomb *et al.*, "Optimizing stability, transport, and divertor operation through plasma shaping for steady-state scenario development in DIII-D," *Phys. of Plasmas*, vol. 16, no. 056116, 2009.